Published in "Acta Materialia 147(): 322–328, 2018"
which should be cited to refer to this work.

Reinforced and superinsulating silica aerogel through in situ cross-linking with silane terminated prepolymers

Subramaniam Iswar [a, f], Geert M.B.F. Snellings [b], Shanyu Zhao [a], Rolf Erni [c], Yeon Kyoung Bahk [d, e], Jing Wang [d, e], Marco Lattuada [f], Matthias M. Koebel [a], Wim J. Malfait [a, *]

[a] *Laboratory for Building Energy Materials and Components, Swiss Federal Laboratories for Materials Science and Technology, Empa, Überlandstrasse 129, 8600 Dübendorf, Switzerland*
[b] *Sustainable Innovation Department, Recticel NV, Damstraat 2, Industriezone 7, 9230 Wetteren, Belgium*
[c] *Electron Microscopy Center, Swiss Federal Laboratories for Materials Science and Technology, Empa, Überlandstrasse 129, 8600 Dübendorf, Switzerland*
[d] *Institute of Environmental Engineering, ETH Zurich, Stefano-Franscini-Platz 3, 8093 Zürich, Switzerland*
[e] *Laboratory for Advanced Analytical Technologies, Swiss Federal Laboratories for Materials Science and Technology, Empa, Überlandstrasse 129, 8600 Dübendorf, Switzerland*
[f] *University of Fribourg, Department of Chemistry, Chemin du Musée 9, 1700 Fribourg, Switzerland*

Keywords:
Natural oil based polyol
Polyurethane
Thermal conductivity
Ormosil
Co-gelation

Silica aerogels have only half the thermal conductivity of conventional insulation, but their application potential is limited by the poor mechanical properties. The fragility arises from the thin necks between the silica nanoparticle building blocks. Here, we produce strong silica aerogels through co-gelation of the polyethoxydisiloxane precursor with a variety of silane terminated prepolymers that reinforce the inter-particle necks, followed by hydrophobization and supercritical CO_2 drying. All prepolymers enabled the synthesis of aerogels with excellent thermal and mechanical properties, but the shortest prepolymer (~2 −3 nm long) yielded the best results. The hybrid aerogels can sustain uniaxial compression without brittle rupture to at least 80% strain for all prepolymer concentrations (5−50 wt%), leading to a final strength of up to 21 MPa, an E modulus up to 3.4 MPa, and an up to 400 times lower dust release rate. In contrast to classical reinforcement strategies, the mechanical improvement does not come with a penalty in thermal conductivity, which remains between 14 and 17 mW m^{-1} K^{-1}. The hybrid aerogels are a unique class of superinsulating materials with superior thermal and mechanical properties and a scalable production process.

1. Introduction

The thermal conductivity (λ) of silica aerogel (12−18 mW m^{-1} K^{-1} under ambient conditions) is only half that of standing air (26 mW m^{-1} K^{-1}) [1–4]. This extreme performance, coupled with their non-flammability, vapour open porosity and recyclability, led to the emergence of a rapidly growing industry for aerogel thermal insulation. In addition to the high cost, the poor mechanical strength, high brittleness and considerable dust release prevent a more widespread use and faster market uptake [5]. It is thus no surprise that researchers worldwide are developing new strategies to improve the mechanical properties of silica aerogels and their corresponding products.

Amongst the earliest polymer-based reinforcement strategies are the classical works by Leventis, Meador and co-workers. These classical X-aerogels [6–18] rely on the in-situ polymerization of a thin conformal coating on the silica surfaces through a post-gelation modification with isocyanate, styrene, epoxy, anhydride or acrylate monomers. Because the reinforcing agents are introduced after the gel has formed, additional solvent exchanges are required to introduce the monomers, particularly if the polymer precursor is not compatible with the gelation solvent, which is most often (m)ethanol or water. X-aerogels display a high compressive modulus (40−900 MPa) and final compressive strength (8−500 MPa), leading to high strength-to-weight ratios. However, these aerogels generally feature high densities

* Corresponding author.
E-mail address: wim.malfait@empa.ch (W.J. Malfait).

(0.25–0.6 g/cm^3) and thermal conductivities (>30 mW m^{-1} K^{-1}) due to the significant mass loading with an additional polymer phase.

A second reinforcement strategy uses co-gelation of a silica precursor or sol with biopolymers [19–22], organically modified silanes (ormosils) [23–25], or silane terminated prepolymers [26–30], and we have selected this last approach in this study. Kramer et al. [26] improved the elasticity of silica aerogel by co-gelation with silanol terminated polydimethylsiloxane chains. Maleki et al. [27] incorporated short tri(m)ethoxysilane terminated linkers into a silica sol that also contained 3-(trimethoxylsilylpropyl) methacrylate. Duan et al. [28,29] reinforced silica aerogels in dimethylformamide by co-gelation with trimethoxy- and triethoxysilane-terminated polyurethane prepolymers, and a similar prepolymer was also used by Gonçalves et al. [30]. Aspen Aerogels described the synthesis of silane-terminated prepolymers through the reaction of di- and triamines with an isocyanatoalkoxysilane and their use as reinforcing agents [31,32]. Jiang et al. [33] prepared polyrotaxane-silica hybrid aerogels with reduced brittleness and increased final strength for a moderate penalty in λ (1–9 mW m^{-1} K^{-1} increase), but most likely underestimated the absolute value of λ through an indirect measurement protocol, resulting for example in an unrealistically low λ value of 10 mW m^{-1} K^{-1} for pure silica aerogel. In nearly all of the above described works, the co-gelation methodology leads to a moderate increase in mechanical strength at the cost of a substantial increase in λ, if λ is reported at all. One notable exception are silica-pectin hybrid aerogels with a strongly increased final compressive strength and E-modulus, but low λ (<18 mW m^{-1} K^{-1}) [21]. However, the silica-pectin synthesis scheme entails long gelation times and additional solvent exchanges prior to hydrophobization and gel drying because of the need for water as a gelation solvent to ensure a good compatibility with the biopolymer. In summary, no direct, scalable synthesis route exist to prepare superinsulating aerogels (λ < 20 mW m^{-1} K^{-1}) with significantly improved mechanical properties.

Here, we introduce strong and superinsulating silica hybrid aerogels with an unprecedented combination of properties, prepared by co-gelation of an ethanol-based silica sol and silane-terminated prepolymers. This route does not depend on a post-gelation modification step typical for classical X-aerogels, but introduces the reinforcement by co-gelation with isocyanatoalkoxysilane based cross-linkers (Fig. 1; Table 1). Because the silane terminated prepolymers are fully compatible with the ethanolic gelation and hydrophobization solvent, no additional solvent exchanges are required.

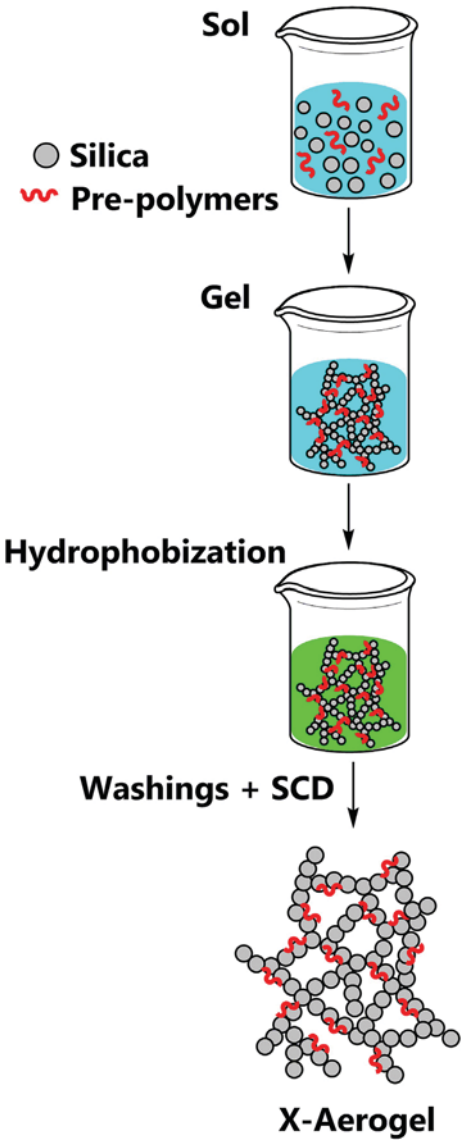

Fig. 1. Synthesis of hybrid aerogels by co-gelation. The length of the polymer chains varies from ~2 to ~100 nm depending on prepolymer type and the diameter of the primary silica particles is ~4 nm.

2. Experimental section

2.1. Synthesis of hybrid aerogels

Hybrid aerogels were prepared by co-gelation of a silica sol with different concentrations of silane terminated prepolymers, described by the prepolymer (X):SiO_2 mass ratio (Fig. 1). The silane-terminated prepolymers are of the general form ($\mathbf{R_1}$O)$_3$-Si-(CH$_2$)$_3$-(NH)-(C=O)-O-$\mathbf{R_2}$-O-(C=O)-(NH)-(CH$_2$)$_3$-Si-(O$\mathbf{R_1}$)$_3$, where $\mathbf{R_1}$ is either a methyl or ethyl group and $\mathbf{R_2}$ can be a short aliphatic chain, a polyether or a natural oil polyol (NOP) based derivative. The prepolymers were either sourced commercially or synthesized by urethane formation between commercial polyols and 3-(triethoxysilyl)propyl isocyanate (Table 1 and Figure S1). In the following, we describe the synthesis procedure using the X = 0.2 hybrid aerogel as an example. The sol was prepared from a mixture of 0.36 g of prepolymer, 9 ml polyethoxydisiloxane (PEDS), a prepolymerized form of tetraethyl orthosilicate (TEOS) containing a water-to-TEOS molar ratio of 1.5 and a SiO_2 content of 20% w/w in ethanol (referred to as PEDS-P$_{750E20}$) [34], 21 ml denatured ethanol (F25-AF-MEK), and 1 ml distilled water prepared under constant stirring for 5–10 min at room temperature. Gelation occurred ca. 10 min after the addition of 0.36 ml 5.5 M NH_4OH in water. The gels were covered with 0.4 ml of ethanol to prevent exposure to the air, and aged at 65 °C for 24 h. The aged gels were hydrophobized by soaking in a mixture of 60 ml hexamethyldisiloxane (HMDSO), 0.24 ml concentrated hydrochloric acid (37%) and 2.2 ml ethanol at 65 °C for 24 h. After 2–4 ethanol washes, the hydrophobized gels were dried in an autoclave (Separex, France) from supercritical CO_2 (SCD).

2.2. Density and nitrogen sorption

The bulk density (ρ_{bulk}) was calculated from the sample mass and envelope volume. The skeletal density ($\rho_{skeletal}$) was obtained from the skeleton volume determined by helium pycnometry (AccuPyc II 1340, Micromeritics). Estimated uncertainties for bulk

Table 1
Properties of prepolymers and corresponding hybrid aerogels (for X:SiO_2 = 0.3:1).

Name	Source	'R2'	MW (g/mol)	λ (mW·m^{-1}·K^{-1})	σ_{max}[a] (MPa)	avg. WCA (°)
*$(MeO)_3$-Si-$(CH_2)_3$-(NH)-(C=O)-O-**R2**-O-(C=O)-(NH)-$(CH_2)_3$-Si-$(OMe)_3$ (commercial)*						
Vestanat® EP-M 95	Evonik	Aliphatic	~600	14.7	6.4	147
Geniosil® STP-E 15	Wacker	Polyether	~11000	17.3	5.2[b]	100
Geniosil® STP-E 35	Wacker	Polyether	~14000	17.4	6.2[b]	113
*$(EtO)_3$-Si-$(CH_2)_3$-(NH)-(C=O)-O-**R2**-O-(C=O)-(NH)-$(CH_2)_3$-Si-$(OEt)_3$ (lab. Synthesized)*						
Empa 2033	Empa	fatty acid dimer diol (Pripol™ 2033, Croda)	~1100	16.6	6.3	133
Empa 1990	Empa	dimer diol (Radianol 1990, Oleon)	~1100	17.0	4.4	144
Empa D-140	Empa	castor-oil derived polyol (Polycin® D-140, Vertellus®)	~1300	16.9	4.6	137
Empa D-265	Empa	castor-oil derived polyol (Polycin® D-265, Vertellus®)	~900	17.0	4.2	138
Empa D-290	Empa	castor-oil derived polyol (Polycin® D-290, Vertellus®)	~900	16.3	3.6	143

[a] Stress at 80% strain.
[b] For X = 0.25 (X:SiO_2); X stands for the mass ratio of prepolymer to silica.

and skeletal density are 5% relative. The specific surface area (S_{BET}) was determined from the nitrogen sorption isotherms (Micromeritics TriFlex) using Brunauer–Emmet–Teller (BET) analysis [35]. The specific pore volume (V_{pore}) was calculated from the bulk and skeletal density of the aerogel ($V_{pore} = (1/\rho_{bulk}) - (1/\rho_{skeletal})$). The average pore diameter was calculated from the specific pore volume and surface area ($D_{pore} = (4V_{pore})/S_{BET}$), rather than the Barrett–Joyner–Halenda (BJH) analysis [36], which for aerogels is affected by mechanical deformation in the desorption branch of the capillary condensation range. In fact, nitrogen desorption can be considered as a second drying of the gel, including a deformation with spring-back [37]. The precision of the BET surface area is around 10 m^2/g, although the accuracy may be lower (~50 m^2/g) as the BET surface area is model and fit dependent. The uncertainties on the pore diameter and specific pore volume are estimated to be on the order of 10%.

2.3. Electron microscopy

Scanning electron microscopy (SEM) images were obtained with a FEI Nova NanoSEM 230 instrument (FEI, Hillsboro, Oregon, USA) at an accelerating voltage of 10 kV and a working distance of 5 mm. The aerogels were fixed on the sample holder using carbon pads and coated with 15–20 nm of platinum before SEM analysis. Transmission electron microscopy (TEM) images were recorded with a JEOL-2200FS microscope operating at an accelerating voltage of 200 kV. The aerogel samples were crushed and dispersed in methanol and the resulting dispersion was drop-cast onto a carbon grid, followed by the evaporation of the methanol at room temperature. TEM images were recorded at magnifications and electron doses suitable to observe the microstructure without causing excessive beam damage. The micrographs shown are representative for the pristine samples where no significant beam modification was noticeable. Beam damage was particularly problematic at higher magnifications due to the increased electron dose.

2.4. NMR, FTIR and elemental analysis

Nuclear Magnetic Resonance (NMR) spectra were collected with magic angle spinning (MAS) on a Bruker Avance III system equipped with a wide-bore 9.4 T magnet, corresponding to Larmor frequencies of 400.2 MHz for ^{1}H, 100.6 MHz for ^{13}C and 79.5 MHz for ^{29}Si. Quantitative solid state ^{1}H spectra of the aerogel samples were collected in 2.5 mm zirconia rotors with a 24 kHz MAS rate to maximize the resolution and with a pulse delay in excess of 5 times the T1 relaxation time to ensure complete relaxation. ^{1}H-^{29}Si cross polarization MAS NMR spectra were recorded with a MAS rate of 4 kHz in 7 mm zirconia rotors to maximize the sensitivity. Fourier Transform Infrared Spectroscopy (FTIR) was carried out on a Bruker Tensor 27 spectrometer. Samples were analysed in attenuated total reflectance (ATR) mode using a diamond crystal. The concentration of carbon, hydrogen and nitrogen was determined by hot gas extraction on a LECO TrueSpec Micro and Oxygen analysis with a LECO RO-478 instrument. The combustion products of carbon (CO_2) and hydrogen (H_2O) were measured with infrared detectors and nitrogen was determined with a katharometer.

2.5. Thermal conductivity, thermogravimetry and uniaxial compression

Thermal conductivity (EN 12667 at 10 °C) was determined from monolithic, square plate specimens with a custom built guarded hot plate device (Figure S2) designed for small samples of low λ materials [38]. Estimated uncertainties for thermal conductivity are 2% relative. Thermogravimetric Analysis (TGA) was investigated on 4–6 mg samples using a Netzsch TGA 209 F1 instrument in 80% v/v O_2 and 20% v/v N_2, and with a heating rate of 5 °C/min from 30 °C to 900 °C. Uniaxial compression tests were performed on monolithic cylindrical samples (10 mm diameter, 20–30 mm high) using a universal mechanical testing setup (Zwick/Z010, Zwick/Roell, Germany), with a 10 kN force transducer (KAP-S, AST Gruppe GmbH, Germany) at 23 °C and 50% RH. Samples were compressed at a rate of 1 mm/min up to 80% strain and elastic moduli were calculated from the linear regime of the compression curves (at 7 ± 3% strain).

2.6. Dust release

Because of the aerogels' fragility and brittleness, standard methods for particle release, for example with a grinding wheel, cannot be applied. As an alternative, a magnetic stirrer with constant rotation rates (100 and 300 rpm) inside a glass flask was used to test the aerogel samples (Figure S3). Air flowing into the chamber was dried and filtered to avoid contamination from the ambient air. Released particles were analysed with two airborne particle measurement systems: a scanning mobility particle sizer (SMPS 3938) which is itself a combination of an electrostatic classifier (3082) and ultrafine condensation particle counter (3776, TSI, USA), and an aerodynamic particle sizer (APS 3321, TSI, USA). The measured ranges of particles were 10–500 nm and 0.54–19.8 μm respectively. Each sample was measured for an hour for each rotation rate, with 2 and 1 min measurement intervals for SMPS and APS, respectively. The sampling flow rate was 1.5 l/min and 1 l/min for SMPS and APS, respectively.

2.7. Water contact angle and humidity uptake

The surface wettability of the samples was evaluated by contact angle measurement, using a Contact Angle System OCA (Data

physics TBU 90E, Germany), combined with a high-speed camera. Water droplets (5 μL) were deposited directly on the top surface of the dried aerogels with a precision stainless steel tip (Gauge 32, EFD). Measurements were repeated for at least 3 different locations on the aerogel surface. The humidity uptake was recorded by reweighting dried samples after exposure to 30, 50 and 80% relative humidity at 25 °C for 7 days. The sample weight was monitored at day 5, 6 and 7 to verify equilibration.

3. Results and discussion

The addition of the prepolymers increases the envelope density (ρ) up to 0.179 g/cm^3 and decreases the specific surface area from 850 to 650 m^2/g (Figure S8 and Table S3), but hybrid aerogels with excellent thermal and mechanical properties can nonetheless be produced from a wide range of silane-terminated prepolymers (Table 1; Figures S4, S5, S6, S7a and S7b). The process is relatively insensitive to the type of prepolymer, as demonstrated by the use of eight different kinds of prepolymers with a wide range of molecular weights and chain lengths, including those from natural oil based polyols (Table 1). However, the EP-M 95 prepolymer, comprised of a short aliphatic chain between the silane terminations, yielded hybrid aerogels with better thermal and mechanical properties, compared to the polyether and NOP based prepolymers. Presumably, the short length of this prepolymer, with a separation of ~2−3 nm between the silane terminations, is optimal to reinforce the inter-particle necks between the primary silica particles (~4 nm diameter) that make up the aerogel backbone (Fig. S13). Longer prepolymer chains somewhat reduce the strengthening capacity, particularly in the case of the NOP based prepolymers (Figures S15 and S16), and lead to higher shrinkage, density and thermal conductivity, particularly for the polyether based prepolymers (Table S3). Note that the variations of the thermal and mechanical properties discussed above are relatively minor compared to the much larger variation in molecular weight (Table 1) and all prepolymers enable the synthesis of hybrid aerogels with excellent thermal and mechanical properties. The reinforcement effect is also not directly proportional to the number of covalent Si-O-Si bonds formed between the prepolymer and silica particles: for example, the addition of the short EP-M-95 prepolymer (MW ~600) instead of the much longer STP-E-35 (MW ~14000) introduces over 20 times more possible covalent crosslinks, but has a similar effect on the maximum stress (σ_{max}) and E modulus, and only leads to a modest difference in thermal conductivity (Table 1, Fig. 5). The aerogels based on the EP-M prepolymer were selected for a more detailed characterization and are discussed in detail below. An extensive description of the data for the other samples can be found in the supplementary information.

3.1. Chemistry and microstructure

The ^{1}H−^{29}Si cross polarization (CP) NMR peak near −66 ppm (T^3) is due to R−Si(−OSi≡)$_3$ groups from fully hydrolysed and condensed prepolymer with a shoulder near −57 ppm (T^2) due to partially condensed R−Si(−OSi≡)$_2$(−OH/OEt) species (Fig. 2) [39], confirming that the prepolymer underwent hydrolysis and condensation, and is incorporated in the aerogel matrix. The successful grafting of the prepolymer is also confirmed by the ^{1}H-^{13}C CP NMR spectra, the quantitative ^{1}H NMR spectra, the ATR-FTIR spectra and the elemental analysis (Figures S9a, 9b, S10; Table S1).

The addition of the prepolymer densifies the microstructure, with a denser packing of both the primary (TEM, Fig. 3a−d) and secondary particles (SEM, Fig. 3e−h), and decreases the size of the mesopores between the secondary particles (Fig. 3e−h), consistent with the pore size analysis (Table S3). The SEM and TEM analysis of the aerogel with the highest prepolymer concentration (X = 1.0) hints at a microstructure that exhibits both silica rich and prepolymer rich domains (Figures S12 and S13), as confirmed by the FTIR spectra (Figure S11). The heterogeneity for this sample may be the result of either an incomplete mixing during sol preparation or a phase separation, and affects some of the bulk properties, e.g. water contact angle or particle release (see below).

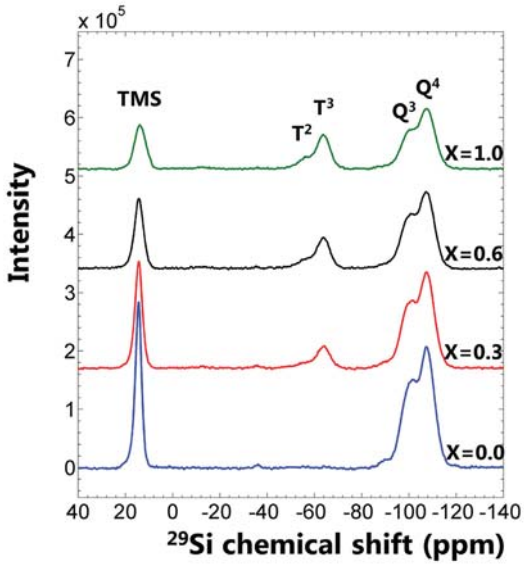

Fig. 2. ^{1}H−^{29}Si cross polarization MAS NMR spectra of EP-M 95 hybrid aerogels.

The hybrid aerogels display nitrogen sorption isotherms with characteristic type IV hysteresis loops (Fig. 4 and Figure S14). The decrease in the width of the hysteresis with increasing prepolymer concentration points at a reduced deformation during BET analysis [37] and provides a first indication of a stiffening/reinforcing effect of the prepolymer.

3.2. Thermal and mechanical properties

All hybrid aerogels can sustain uniaxial compression without rupture to at least 80% strain (Fig. 5a, Figures S15, and S16), regardless of the prepolymer type or concentration, and can be recovered as a cohesive, flattened disk after testing. In contrast, prepolymer free reference silica aerogel typically breaks up into multiple small pieces below 50% strain. The addition of prepolymers increases the compressive (E) modulus, compressive strength at 10% and 50% strain (σ_{10}, σ_{50}) and final compressive strength (σ_{max}), which corresponds to the strength at 80% for the hybrid aerogels as none of them failed at lower strain (Fig. 5b and c, Figures S17a-d and S18a-d). The increase in σ_{max} is a linear function of the prepolymer concentration (Fig. 5b), whereas the E modulus follows a power-law dependence on sample density (Figure S19; Tables S2 and S3). The hybrid aerogels prepared with the EP-M 95 prepolymer exhibit the best mechanical performance with a final compressive strength as high as 21 MPa and an E modulus of up to 3.4 MPa. Remarkably, the EP-M 95 derived materials also display the lowest thermal conductivities with λ between 14.7 and 16.8 mW m^{-1} K^{-1} for densities in the 0.10 and 0.18 g/cm^3 range (Fig. 5d). The thermal conductivity displays a minimum in λ around X~0.4 and ρ~0.12 g/cm^3, consistent with the well-known dependence of λ on ρ for silica aerogels [2,4] (Fig. 5d and Figure S8; Table S3). At lower prepolymer

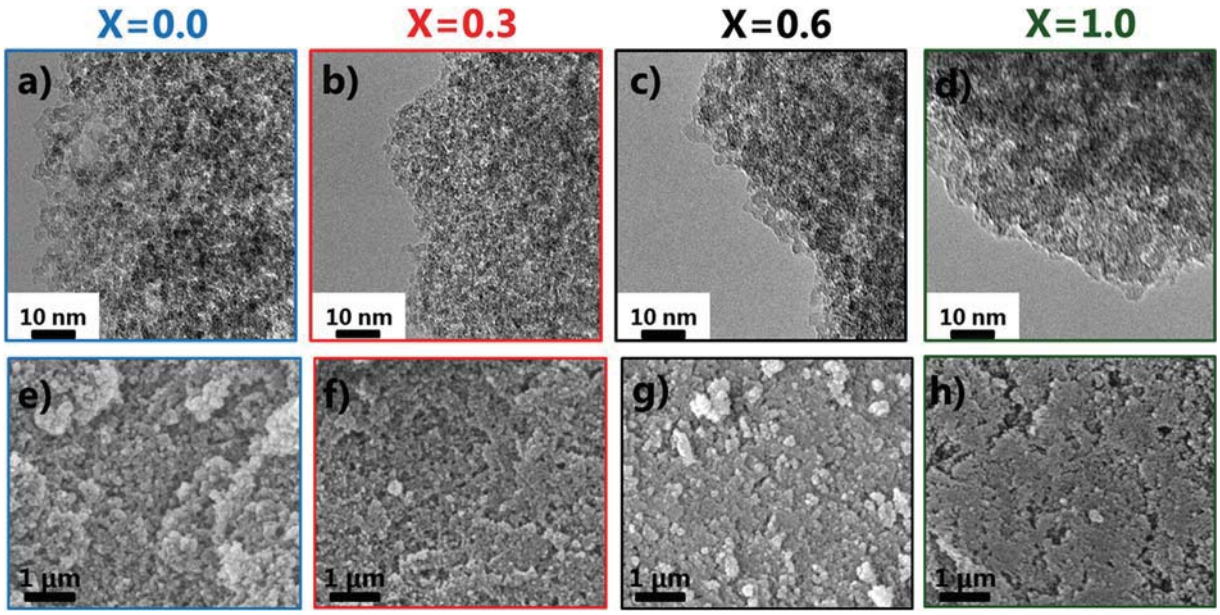

Fig. 3. Microstructure of EP-M 95 hybrid aerogels: TEM images for (a) X = 0.0 (i.e. reference silica aerogel), (b) X = 0.3, (c) X = 0.6, (d) X = 1.0 (i.e. a 1:1 prepolymer:SiO_2 mass ratio); (e–h) SEM images for the same prepolymer concentrations.

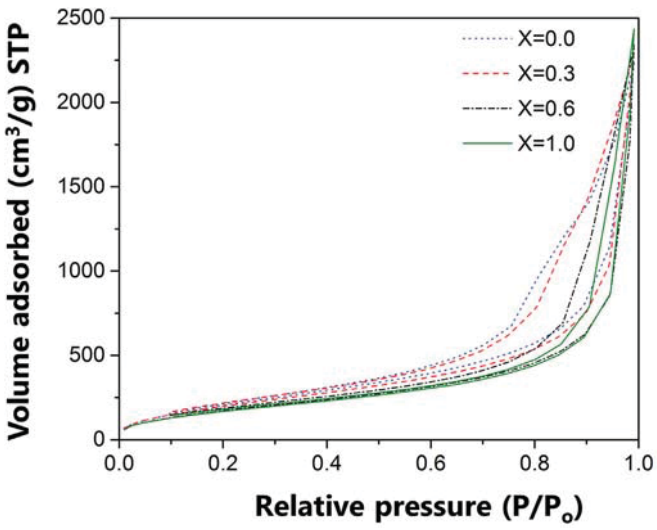

Fig. 4. Nitrogen sorption isotherms of EP-M 95 hybrid aerogels.

concentrations and densities, the gas phase conduction is higher because of larger pores. At higher prepolymer loadings and densities, the solid conduction through the skeleton increases, even though this increase is minimal for the EP-M 95 based hybrid aerogels.

The ability to improve silica aerogel's mechanical properties without a penalty in thermal conductivity positions this new class of polymer modified ormosil/silica aerogels at the leading edge of what is possible in aerogel reinforcement (Fig. 6). Indeed, previous reinforcement strategies have consistently increased thermal conductivity, negating the unique selling point of aerogels as thermal superinsulation materials, with only one exception, the pectin-silica hybrid aerogels recently developed in our laboratory [21]. Compared to the latter, the materials presented here use a simpler, more scalable production processes, with faster gelation times and fewer solvent exchanges.

3.3. Dust release

The reduced brittleness of EP-M 95 containing aerogels is reflected in the dust release during abrasion, which is nearly eliminated, with a reduction by a factor of 400 compared to reference silica aerogel. The optimum prepolymer:SiO_2 ratio with respect to particle release is X = 0.6 (Fig. 5e, Figures S20a-d and S21). The decrease in particle release with increasing prepolymer loading between X = 0 and X = 0.6 can be readily explained by the improved mechanical properties, and reduced brittleness in particular, with increasing prepolymer loading. The higher dust release for the highest prepolymer concentration (X = 1.0) despite its higher final compressive strength is more surprising, but may stem from the existence of silica rich domains inferred from the TEM, SEM and FTIR analysis (Figures S11-S13).

3.4. Thermal stability and humidity uptake

In addition to the outstanding thermal, mechanical and dust release properties, the EP-M 95 materials are stable up to 240 °C, as confirmed by thermogravimetric analysis (Figure S22). Because of the silylation treatment, the hybrid aerogels are hydrophobic with a low humidity uptake (<2 wt % at 80% relative humidity, Figure S23) and the water contact angle is not significantly affected (>135°) by the addition of prepolymer for all but the highest prepolymer concentration (Fig. 4f and Figure S27; Table S3). The water contact angles (Table 1, Fig. 5f, Figures S29, S30; Table S3), but not the humidity uptake (Figures S25 and S26), are more strongly affected for the hybrid aerogels from polyether-based prepolymers (STP-E 15 and STP-E 35).

4. Conclusions

Mechanically strong, superinsulating aerogels are produced by a one-step sol-gel process. In contrast to other reinforcement strategies, no additional solvent exchanges or post-modification steps, compared to standard silica aerogel synthesis, are required. The ability to produce materials with improved

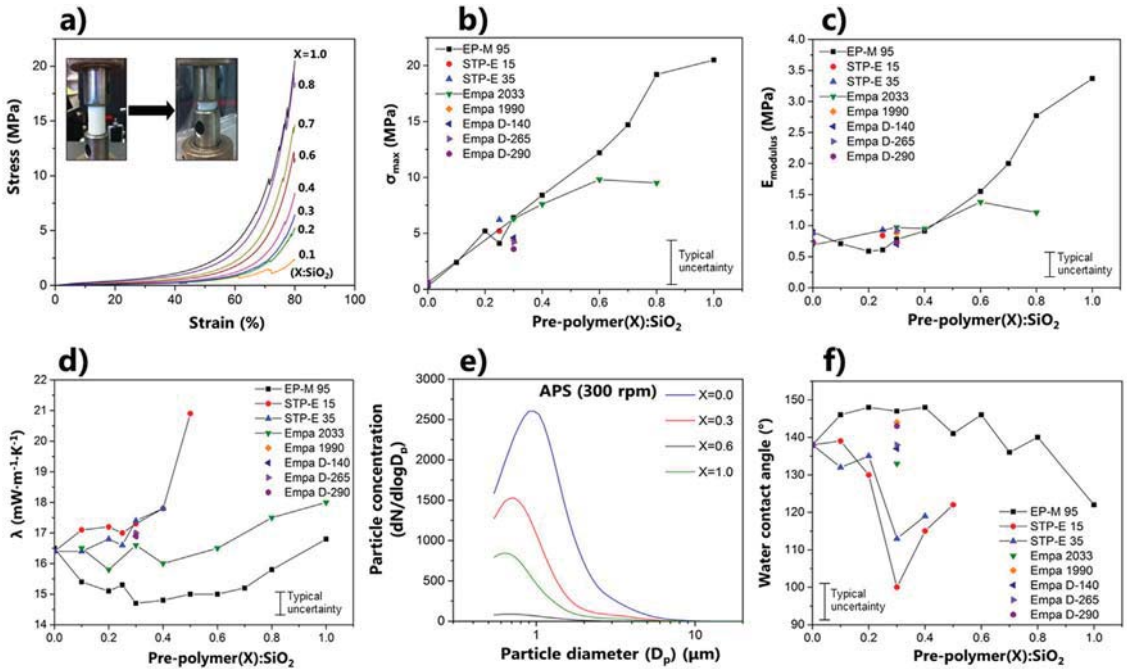

Fig. 5. (a) Stress-strain curves of EP-M 95 hybrid aerogels for variable prepolymer concentrations; (b) Final compressive strength (σ_{max}); (c) E modulus; (d) λ; (e) Particle release of EP-M 95 hybrid aerogels (300 rpm, APS - 0.54–19.8 μm); and (f) Water contact angle. Note that the hybrid aerogels with Empa 1990, Empa D-140, Empa D-265 and Empa D-290 prepolymers were synthesized for only one concentration (X = 0.3).

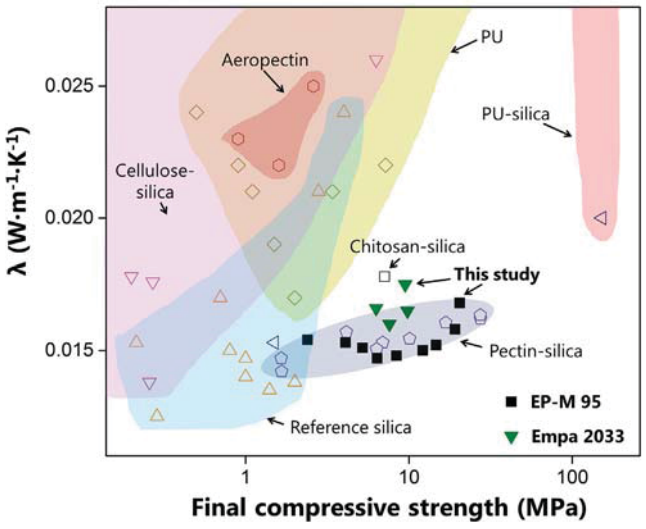

Fig. 6. λ versus final compressive strength for aerogel-like materials: [4,8,11,15,16,21,22,40–45]. Data on the polyrotaxane-silica hybrids [33] were not included because λ was determined indirectly.

properties from a wide variety of prepolymers, including those from renewable precursors, highlights the flexibility of the approach. The reinforced, hydrophobic hybrid aerogel materials can sustain uniaxial compression to at least 80% strain, display a high compressive strength and stiffness and have all but eliminated the particle release. Crucially, the reinforced aerogels maintain the ultra-low thermal conductivity typical for silica aerogel (15–17 mW m^{-1} K^{-1}). This new class of polymer modified ormosil/silica aerogels offer a superior insulation performance, when compared to the current state-of-the-art, and uses a simpler and more scalable production process.

Acknowledgements

The authors are grateful to the Flemish agency 'Agentschap Innoveren en Ondernemen' for providing financial support of this research. The NMR hardware was partially funded by the Swiss National Science Foundation under Grant No. 206021_150638/1. We thank Beatrice Fischer for her help with TGA, FTIR analysis and uniaxial compression tests. Samples of Vestanat® EP-M 95 (Evonik), Geniosil® STP-E 15, Geniosil® STP-E 35 (Wacker), PripolTM 2033 (Croda), Radianol 1990 (Oleon), Polycin® D-140, Polycin® D-265 and Polycin® D-290 (Vertellus Performance Materials Inc.) were kindly provided by the respective suppliers.

Appendix A. Supplementary data

Supplementary data related to this article can be found at https://doi.org/10.1016/j.actamat.2018.01.031.

References

[1] S.S. Kistler, Coherent expanded aerogels and jellies, Nature 127 (1931) 741, https://doi.org/10.5254/1.3539386, 741.

[2] N. Hüsing, U. Schubert, Aerogels—airy materials: chemistry, structure, and properties, Angew. Chem. Int. Ed. 37 (1998) 22–45, https://doi.org/10.1002/1521-3773(19980202)37:1/2<22::AID-ANIE22>3.3.CO;2–9.

[3] M.A. Aegerter, N. Leventis, M.M. Koebel, Aerogels Handbook, Springer, New York, 2011.

[4] J.C.H. Wong, H. Kaymak, S. Brunner, M.M. Koebel, Mechanical properties of monolithic silica aerogels made from polyethoxydisiloxanes, Microporous Mesoporous Mater. 183 (2014) 23–29, https://doi.org/10.1016/j.micromeso.2013.08.029.

[5] T. Woignier, J. Phalippou, Mechanical strength of silica aerogels, J. Non-Cryst. Solids 100 (1988) 404–408, https://doi.org/10.1016/0022-3093(88)90054-3.

[6] N. Leventis, C. Sotiriou-Leventis, G. Zhang, A.-M.M. Rawashdeh, Nanoengineering strong silica aerogels, Nano Lett. 2 (2002) 957–960, https://doi.org/10.1021/nl025690e.

[7] G. Zhang, A. Dass, A.-M.M. Rawashdeh, J. Thomas, J.A. Counsil, C. Sotiriou-Leventis, E.F. Fabrizio, F. Ilhan, P. Vassilaras, D.A. Scheiman, L. McCorkle, A. Palczer, J.C. Johnston, M.A. Meador, N. Leventis, Isocyanate-crosslinked silica aerogel monoliths: preparation and characterization, J. Non-Cryst. Solids

350 (2004) 152–164, https://doi.org/10.1016/j.jnoncrysol.2004.06.041.
[8] A. Katti, N. Shimpi, S. Roy, H. Lu, E.F. Fabrizio, A. Dass, L.A. Capadona, N. Leventis, Chemical, physical, and mechanical characterization of isocyanate cross-linked amine-modified silica aerogels, Chem. Mater. 18 (2006) 285–296, https://doi.org/10.1021/cm0513841.
[9] L.A. Capadona, M.A.B. Meador, A. Alunni, E.F. Fabrizio, P. Vassilaras, N. Leventis, Flexible, low-density polymer crosslinked silica aerogels, Polym. Prepr. (Am. Chem. Soc., Div. Polym. Chem.) 47 (2006) 5754–5761, https://doi.org/10.1016/j.polymer.2006.05.073.
[10] M.A.B. Meador, E.F. Fabrizio, F. Ilhan, A. Dass, G. Zhang, P. Vassilaras, J.C. Johnston, N. Leventis, Cross-linking amine-modified silica aerogels with epoxies: mechanically strong lightweight porous materials, Chem. Mater. 17 (2005) 1085–1098, https://doi.org/10.1021/cm048063u.
[11] M.A.B. Meador, L.A. Capadona, L. McCorkle, D.S. Papadopoulos, N. Leventis, Structure–Property relationships in porous 3D nanostructures as a function of preparation conditions: isocyanate cross-linked silica aerogels, Chem. Mater. 19 (2007) 2247–2260, https://doi.org/10.1021/cm070102p.
[12] B.N. Nguyen, M.A.B. Meador, A. Medoro, V. Arendt, J. Randall, L. McCorkle, B. Shonkwiler, Elastic behavior of methyltrimethoxysilane based aerogels reinforced with tri-isocyanate, ACS Appl. Mater. Interfaces 2 (2010) 1430–1443, https://doi.org/10.1021/am100081a.
[13] S.L. Vivod, M.A.B. Meador, B.N. Nguyen, R. Perry, Di-isocyanate cross-linked silica aerogels with hexyl links incorporated into the underlying silica backbone, Polym. Prepr. (Am. Chem. Soc., Div. Polym. Chem.) 50 (2009) 119–120.
[14] L.A. Capadona, M.A. Meador, Process for Preparing Polymer Reinforced Silica Aerogels, US 8,067,478 B1, 2011.
[15] K.-J. Chang, Y.-Z. Wang, K.-C. Peng, H.-S. Tsai, J.-R. Chen, C.-T. Huang, K.-S. Ho, W.-F. Lien, Preparation of silica aerogel/polyurethane composites for the application of thermal insulation, J. Polym. Res. 21 (2014) 338, https://doi.org/10.1007/s10965-013-0338-7.
[16] G. Churu, B. Zupančič, D. Mohite, C. Wisner, H. Luo, I. Emri, C. Sotiriou-Leventis, N. Leventis, H. Lu, Synthesis and mechanical characterization of mechanically strong, polyurea-crosslinked, ordered mesoporous silica aerogels, J. Sol. Gel Sci. Technol. 75 (2015) 98–123, https://doi.org/10.1007/s10971-015-3681-9.
[17] F. Ilhan, E.F. Fabrizio, L. McCorkle, D.A. Scheiman, A. Dass, A. Palczer, M.B. Meador, J.C. Johnston, N. Leventis, Hydrophobic monolithic aerogels by nanocasting polystyrene on amine-modified silica, J. Mater. Chem. 16 (2006) 3046, https://doi.org/10.1039/b604323b.
[18] H. Maleki, L. Durães, A. Portugal, Synthesis of mechanically reinforced silica aerogels via surface-initiated reversible addition-fragmentation chain transfer (RAFT) polymerization, J. Mater. Chem. 3 (2015) 1594–1600, https://doi.org/10.1039/C4TA05618C.
[19] M.R. Ayers, A.J. Hunt, Synthesis and properties of chitosan-silica hybrid aerogels, J. Non-Cryst. Solids 285 (2001) 123–127, https://doi.org/10.1016/S0022-3093(01)00442-2.
[20] Q. Ma, Y. Liu, Z. Dong, J. Wang, X. Hou, Hydrophobic and nanoporous chitosan-silica composite aerogels for oil absorption, J. Appl. Polym. Sci. 132 (2015) 1–11, https://doi.org/10.1002/app.41770.
[21] S. Zhao, W.J. Malfait, A. Demilecamps, Y. Zhang, S. Brunner, L. Huber, P. Tingaut, A. Rigacci, T. Budtova, M.M. Koebel, Strong, thermally superinsulating biopolymer-silica aerogel hybrids by cogelation of silicic acid with pectin, Angew. Chem. Int. Ed. 54 (2015) 14282–14286, https://doi.org/10.1002/anie.201507328.
[22] S. Zhao, W.J. Malfait, E. Jeong, B. Fischer, Y. Zhang, H. Xu, E. Angelica, W.M. Risen, J.W. Suggs, M.M. Koebel, Facile one-pot synthesis of mechanically robust biopolymer-silica nanocomposite aerogel by cogelation of silicic acid with chitosan in aqueous media, ACS Sustain. Chem. Eng. 4 (2016) 5674–5683, https://doi.org/10.1021/acssuschemeng.6b01574.
[23] F. Schwertfeger, W. Glaubitt, U. Schubert, Hydrophobic aerogels from Si(OMe)4/MeSi(OMe)3 mixtures, J. Non-Cryst. Solids 145 (1992) 85–89, https://doi.org/10.1016/S0022-3093(05)80435-1.
[24] N. Huesing, U. Schubert, K. Misof, P. Fratzl, Formation and structure of porous gel networks from Si(OMe)4 in the presence of a(CH2)nSi(OR)3 (A = functional group), Chem. Mater. 10 (1998) 3024–3032.
[25] K. Kanamori, Organic–inorganic hybrid aerogels with high mechanical properties via organotrialkoxysilane-derived sol–gel process, J. Ceram. Soc. Japan 119 (2011) 16–22, https://doi.org/10.2109/jcersj2.119.16.
[26] S.J. Kramer, F. Rubio-Alonso, J.D. Mackenzie, Organically modified silicate aerogels, "Aeromosils", Mater. Res. Soc. 435 (1996) 295–300.
[27] H. Maleki, L. Durães, A. Portugal, Synthesis of lightweight polymer-reinforced silica aerogels with improved mechanical and thermal insulation properties for space applications, Microporous Mesoporous Mater. 197 (2014) 116–129, https://doi.org/10.1016/j.micromeso.2014.06.003.
[28] Y. Duan, S.C. Jana, B. Lama, M.P. Espe, Reinforcement of silica aerogels using silane-end-capped polyurethanes, Langmuir 29 (2013) 6156–6165, https://doi.org/10.1021/la4007394.
[29] Y. Duan, S.C. Jana, B. Lama, M.P. Espe, Self-crosslinkable poly(urethane urea)-reinforced silica aerogels, RSC Adv. 5 (2015) 71551–71558, https://doi.org/10.1039/C5RA11769K.
[30] L.F.F.F. Gonçalves, C.J.R. Silva, F.K. Kanodarwala, J.A. Stride, M.R. Pereira, M.J.M. Gomes, Synthesis and characterization of organic-inorganic hybrid materials prepared by sol-gel and containing ZnxCd1-xS nanoparticles prepared by a colloidal method, J. Lumin. 144 (2013) 203–211, https://doi.org/10.1016/j.jlumin.2013.07.011.
[31] L.O. Duan, G.L. Gould, Ormosil Aerogels Containing Silicon Bonded Linear Polymers, US 2005/0192367 A1, 2005.
[32] G. Gould, D. Ou, R. Begag, W. Rhine, Highly-transparent polymer modified silica aerogels, Polym. Prepr. (Am. Chem. Soc., Div. Polym. Chem.) 49 (2008) 534–535.
[33] L. Jiang, K. Kato, K. Mayumi, H. Yokoyama, K. Ito, One-pot synthesis and characterization of polyrotaxane – silica hybrid aerogel, ACS Macro Lett. 6 (2017) 281–286, https://doi.org/10.1021/acsmacrolett.7b00014.
[34] G.M. Pajonk, E. Elaloui, P. Achard, B. Chevalier, J.-L. Chevalier, M. Durant, Physical properties of silica gels and aerogels prepared with new polymeric precursors, J. Non-Cryst. Solids 186 (1995) 1–8, https://doi.org/10.1016/0022-3093(95)00210-3.
[35] S. Brunauer, P.H. Emmett, E. Teller, Adsorption of gases in multimolecular layers, J. Am. Chem. Soc. 60 (1938) 309–319, https://doi.org/10.1021/ja01269a023 doi:citeulike-article-id:4074706\r.
[36] E.P. Barrett, L.G. Joyner, P.P. Halenda, The determination of pore volume and area distributions in porous substances. I. Computations from nitrogen isotherms, J. Am. Chem. Soc. 73 (1951) 373–380, https://doi.org/10.1021/ja01145a126.
[37] G. Reichenauer, Structural characterization of aerogels, in: M.A. Aegerter, N. Leventis, M.M. Koebel (Eds.), Aerogels Handbook, Springer, New York, 2011, pp. 449–498, https://doi.org/10.1007/978-1-4419-7589-8.
[38] T. Stahl, S. Brunner, M. Zimmermann, K. Ghazi Wakili, Thermo-hygric properties of a newly developed aerogel based insulation rendering for both exterior and interior applications, Energy Build. 44 (2012) 114–117, https://doi.org/10.1016/j.enbuild.2011.09.041.
[39] W.J. Malfait, R. Verel, M.M. Koebel, Hydrophobization of silica aerogels: insights from quantitative solid-state NMR spectroscopy, J. Phys. Chem. C 118 (2014) 25545–25554, https://doi.org/10.1021/jp5082643.
[40] C. Rudaz, R. Courson, L. Bonnet, S. Calas-Etienne, H. Sallée, T. Budtova, Aeropectin: fully biomass-based mechanically strong and thermal superinsulating aerogel, Biomacromolecules 15 (2014) 2188–2195, https://doi.org/10.1021/bm500345u.
[41] J. Cai, S. Liu, J. Feng, S. Kimura, M. Wada, S. Kuga, L. Zhang, Cellulose-silica nanocomposite aerogels by in-situ formation of silica in cellulose gel, Angew. Chem. Int. Ed. 51 (2012) 2076–2079, https://doi.org/10.1002/anie.201105730.
[42] A. Demilecamps, C. Beauger, C. Hildenbrand, A. Rigacci, T. Budtova, Cellulose-silica aerogels, Carbohydr. Polym. 122 (2015) 293–300, https://doi.org/10.1016/j.carbpol.2015.01.022.
[43] S. Zhao, Z. Zhang, G. Sèbe, R. Wu, R.V. Rivera Virtudazo, P. Tingaut, M.M. Koebel, Multiscale assembly of superinsulating silica aerogels within silylated nanocellulosic scaffolds: improved mechanical properties promoted by nanoscale chemical compatibilization, Adv. Funct. Mater. 25 (2015) 2326–2334, https://doi.org/10.1002/adfm.201404368.
[44] C. Chidambareswarapattar, P.M. McCarver, H. Luo, H. Lu, C. Sotiriou-Leventis, N. Leventis, Fractal multiscale nanoporous polyurethanes: flexible to extremely rigid aerogels from multifunctional small molecules, Chem. Mater. 25 (2013) 3205–3224, https://doi.org/10.1021/cm401623h.
[45] N. Diascorn, S. Calas, H. Sallée, P. Achard, A. Rigacci, Polyurethane aerogels synthesis for thermal insulation - textural, thermal and mechanical properties, J. Supercrit. Fluids 106 (2015) 76–84, https://doi.org/10.1016/j.supflu.2015.05.012.